Journal of The Electrochemical Society, **157** (3) D127-D134 (2010)
0013-4651/2010/157(3)/D127/8/$28.00 © The Electrochemical Society

Effects of Additives on Cu-MWCNT Composite Plating Films

Susumu Arai,[a,*,z] Takashi Saito,[a] and Morinobu Endo[b]

[a]*Department of Chemistry and Material Engineering and* [b]*Department of Electrical and Electronic Engineering, Faculty of Engineering, Shinshu University, Nagano 380-8553, Japan*

The effects of plating bath additives on copper-multiwalled carbon nanotube (MWCNT) composite platings were studied. An acidified cupric sulfate electrolyte containing MWCNTs and polyacrylic acid as a dispersing agent was used as the base plating bath. Chloride ions (Cl^-), poly(ethylene glycol), bis(3-sulfopropyl)disulfide (SPS), and Janus green B (JGB) were examined as additives. The surface morphologies and cross-sectional microstructures of the electrodeposited films were investigated, and the MWCNT content of the films was determined. Furthermore, the electrical resistivity and field emission properties of the films were evaluated. The simultaneous addition of Cl^-, SPS, and JGB to the base plating bath was effective for forming smooth Cu-MWCNT composite films with a high MWCNT content over a wider range of current densities. The optimal bath composition was 0.85 mol dm^{-3} $CuSO_4 \cdot 5H_2O$ + 0.55 mol dm^{-3} H_2SO_4 + 100 ppm PA5000 + 2 g dm^{-3} MWCNTs + 2 ppm SPS + 2 ppm JGB +50 ppm Cl^-. Cu-MWCNT composite films containing 0.15–0.33 mass % MWCNTs with smooth surface morphologies were formed in the current density range of 0.5–5 A dm^{-2}. The electrical resistivity of the films was around 2 $\mu\Omega$ cm, and they showed obvious field emission properties.
 [DOI: 10.1149/1.3274202]

Manuscript submitted September 7, 2009; revised manuscript received November 17, 2009. Published January 12, 2010.

Carbon nanotubes (CNTs)[1,2] have excellent mechanical characteristics, such as high tensile strength and elastic modulus. They also show high thermal and electrical conductivities. In addition, they possess high aspect ratios (length to diameter), a sharp tip curvature, and chemical inertness. Research into practical applications of CNTs, such as the preparation of resin-CNT, ceramic-CNT, and metal-CNT composites, has been actively pursued. Recently, the fabrication of metal-CNT composites has been attempted using plating techniques.[3-11]

Copper plating is widely used in the electronics industry mainly due to its superior electrical and thermal conductivity. In particular, developments in "via-filling" techniques for printed circuit boards and "superfilling" for the damascene process by copper electrodeposition have been vigorously advanced.[12-27]

The present authors as well as others have reported that Cu-CNT composites can be electrodeposited, though the deposits tend to form bumpy[28-30] or powdery[31] morphologies, owing to the intrinsic and unique electrical conduction of CNTs.[32] Because CNTs possess electrical conductivity only in the axial direction, once one end of a CNT is incorporated in the deposited copper matrix, the electrodeposition of copper occurs not only on the deposited copper matrix but also on the other protruding end of the CNT. As electrodeposition proceeds, CNTs become incorporated into the deposited copper on the protruding end of the CNT, resulting in bumpy or powdery morphologies.[28-31] We have also reported that the Cu-CNT composite films showed superior field emission properties such as a lower turn-on electric field.[33] To make a Cu-CNT composite plating technology practicable for the industry, extending the range of current densities in which Cu-CNT composite films with smooth surfaces and a higher CNT content are formed is essential. In general, the addition of suitable additives to the plating bath is an effective method for forming plating films with smooth surface morphologies and compact microstructures over a wider current density range.

In this study, the effects of additives that are typically used for the via-filling or superfilling on surface morphologies and microtextures of the electrodeposited Cu-CNT composite films were studied. The electrical resistivity and the field emission properties of these films were also evaluated.

Experimental

The CNTs used in the present study are commercially available vapor-grown multiwalled carbon nanotubes (MWCNTs, Showa Denko Co. Ltd.) formed via catalyst-assisted chemical vapor deposition[34] and heat-treated at 2800°C in an argon gas atmosphere for 30 min. The MWCNTs were typically of 150 nm diameter and 15 μm length. A sulfuric copper plating bath (0.85 mol dm^{-3} $CuSO_4 \cdot 5H_2O$ + 0.55 mol dm^{-3} H_2SO_4) was used as the base bath. The MWCNTs did not disperse uniformly in the base bath; therefore, a homogeneous dispersion of MWCNTs was achieved by the addition of a polyacrylic acid (mean molecular weight 5000; PA5000) dispersant[7-11,28-31,33] to the base bath with stirring. The composition of the base Cu-MWCNT composite plating bath used in the present study was 0.85 mol dm^{-3} $CuSO_4 \cdot 5H_2O$ + 0.55 mol dm^{-3} H_2SO_4 + 100 ppm PA5000 + 2 g dm^{-3} MWCNTs. As shown in Table I, 50 ppm chloride ions (HCl), 100 ppm poly(ethylene glycol) with 2000 mean molecular weight (PEG2000), 2 ppm bis(3-sulfopropyl)disulfide (SPS), and 2 ppm Janus green B (JGB) were added to the base Cu-MWCNT composite plating bath as additives to prepare various composite plating baths. A commercially available electrolytic cell (Microcell model I, Yamamoto-Ms Co. Ltd.) with internal dimensions of 65 × 65 × 95 mm was employed for the electrodeposition. The volume of the plating bath was 250 cm^3. A pure copper plate with an exposed surface area of 10 cm^2 (3 × 3.33 cm) was used as the substrate. A copper plate containing a small amount of phosphorus was used as the anode. The electrodeposition was performed under galvanostatic conditions in the current density range of 0.5–5 A dm^{-2} with agitation by bubbling air. This agitation was effective to suppress the sedimentation of MWCNTs, that is, to homogeneously disperse MWCNTs in the plating bath. The Microcell model I mentioned above has holes at the bottom for the air used for agitation, and the air bubbling was conducted using an exclusive air pump (Hull Cell Air Pump, Yamamoto-Ms Co. Ltd.). The bath temperature was 25°C.

The cathodic polarization curves were measured using an electrochemical measurement system (Hokuto Denko HZ-5000). A platinum plate, a copper plate, and a saturated calomel electrode were used as the working, counter, and reference electrodes, respectively. Measurements were carried out with air bubbling using the electrolytic cell mentioned above. The microstructures of the Cu-MWCNT composite films were examined using a field-emission type scanning electron microscope (JEOL JSM-7000F). An exclusive sample preparation equipment (cross section polisher; JEOL SM-09010) was used to prepare cross-sectional samples for observations. The MWCNT content in the composite films was determined by direct weighing. For the weight measurement, thick Cu-MWCNT composite films (over 8 g) were electrodeposited. Subsequently, the copper matrix of the films was dissolved in nitric acid. The MWCNTs in the nitric acid solution were then filtered, dried, and weighed. The electrical resistivity of the composite films was investigated using a four-terminal method (a four-point probe system) after removing the

* Electrochemical Society Active Member.
z E-mail: araisun@shinshu-u.ac.jp

Table I. Bath compositions.

Reagents	Bath A	Bath B	Bath C	Bath D	Bath E	Bath F	Bath G	Bath H
$CuSO_4 \cdot 5H_2O$ (mol dm^{-3})	0.85	0.85	0.85	0.85	0.85	0.85	0.85	0.85
H_2SO_4 (mol dm^{-3})	0.55	0.55	0.55	0.55	0.55	0.55	0.55	0.55
PA5000 (ppm)	100	100	100	100	100	100	100	100
PEG2000 (ppm)	100							
SPS (ppm)	2	2			2	2		2
JGB (ppm)	2		2		2		2	2
Cl^- (HCl) (ppm)	50			50		50	50	50
CNTs (g dm^{-3})	2	2	2	2	2	2	2	2

stainless steel substrate. Field emission properties were measured using a diode-type field emission measurement system (ULVAC CN-EMS30). The base pressure of the field emission chamber was around 10^{-5} Pa. The gap between the anode and the film surface was 1 mm.

Results and Discussion

Figure 1 shows surface scanning electron microscopy (SEM) images of composite films electrodeposited at two different current densities from the base Cu-MWCNT composite plating bath. A relatively flat surface morphology is seen at 1 A dm^{-2} (a similar morphology is also seen at 0.5 A dm^{-2}), whereas a bumpy and spherical morphology is observed at 5 A dm^{-2}. The bumpy morphology is due to the unique electrical conduction properties of MWCNTs, as described above. Compelling evidence for this has been reported in our previous paper.[31]

Figure 2 shows schematic illustrations of the growth processes of the Cu-MWCNT composite films at two different current densities.[30] When the current density is relatively low, at 1 A dm^{-2} in the present study, copper electrodeposits onto the substrate, trapping and embedding MWCNTs in the depositing copper matrix, resulting in a relatively smooth surface morphology (Fig. 2a). However, in the higher current density, at 5 A dm^{-2} in the present study, the MWCNTs are first incorporated into the deposited copper matrix. Then, copper electrodeposits not only onto the existing copper matrix but also on the protruding tips of the incorporated MWCNTs in the deposited copper matrix. Newly arrived MWCNTs are then incorporated into the latter copper regions, resulting in a bumpy surface morphology (Fig. 2b). If defects such as vacancies exist on the outer surface of the MWCNTs, copper might also be electrodeposited onto these regions. However, in this study, we assume that no defects exist on the outer surface of the MWCNTs. The electrodeposition of copper onto the end of an MWCNT easily occurs at higher current densities, that is, at a more negative potential.[30] To form smooth and compact Cu-MWCNT composite films containing sufficient amounts of MWCNTs over a wider range of current densities, the addition of various additives to the base Cu-MWCNT composite plating bath was examined.

Figure 3 shows surface SEM images of composite films electrodeposited at various current densities from bath A (base Cu −MWCNT composite plating + 100 ppm PEG2000 + 2 ppm SPS + 2 ppm JGB + 50 ppm Cl^-). This combination of additives has been commonly used for via-filling or superfilling.[13,14,16,20,21] Although smooth surface morphologies were obtained, MWCNTs were barely observed in the films. This shows that the simple addition of a typical combination of additives does not yield ideal Cu-MWCNT composite films. Bath A had a smaller dispersion of MWCNTs compared to the other composite plating baths based on visual observation. The smaller dispersion of MWCNTs means that the MWCNTs formed large secondary particles in the plating bath. Therefore, the combined addition of PEG2000, SPS, JGB, and Cl^- to the base Cu-MWCNT composite bath reduced the dispersion of MWCNTs, resulting in a smaller content of MWCNTs in the deposited film. PA5000 has carboxyl groups, and PEG2000 has hydroxyl

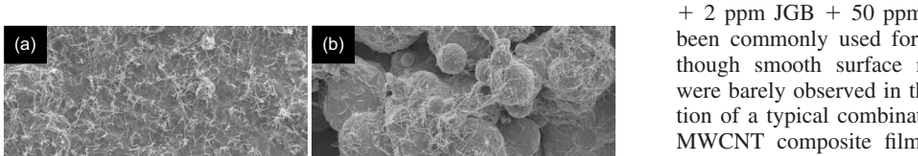

Figure 1. Surface SEM images of Cu-MWCNT composite films electrodeposited from the base Cu-MWCNT composite plating bath at current densities of (a) 1 and (b) 5 A dm^{-2}.

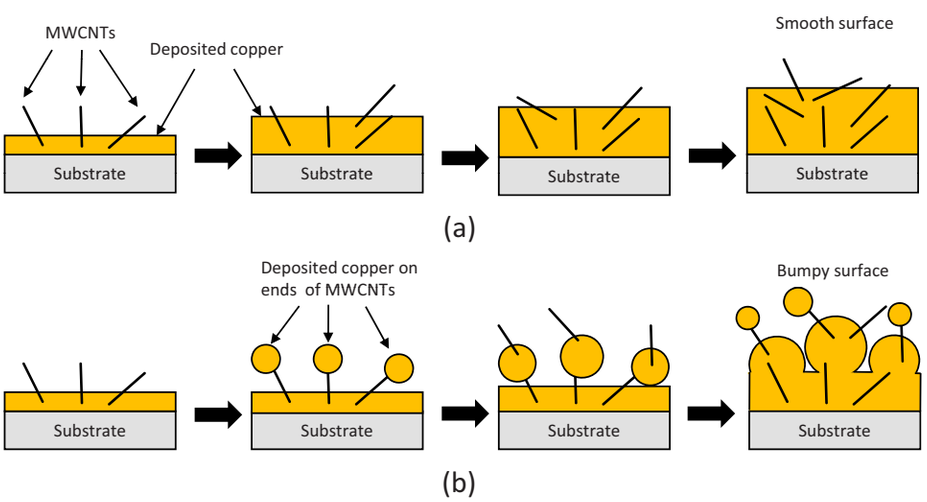

Figure 2. (Color online) Schematic illustrations of the growth processes of the Cu-MWCNT composite films (a) at a low current density (1 A dm^{-2}) and (b) at a high current density (5 A dm^{-2}).

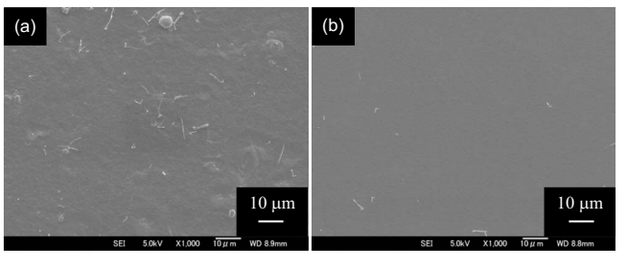

Figure 3. Surface SEM images of Cu-MWCNT composite films electrodeposited from bath A at current densities of (a) 0.5 and (b) 5 A dm^{-2}.

groups. Liu et al. reported the esterification reaction between alcohols and organic acids in damascene copper electropolishing.[35] It might be considered that the addition of PEG2000 to the base Cu-MWCNT composite plating bath changed the PA5000 dispersant, resulting in a lower dispersion of MWCNTs and less amount of MWCNTs in the deposits. In any case, bath A is not suitable for Cu-MWCNT composite plating, and consequently, an individual or combined addition of additives without PEG2000 was examined.

Figure 4 shows surface SEM images of the composite films electrodeposited at different current densities from baths B, C, and D, which contain SPS, JGB, and Cl^-, respectively, as additives. At 1 A dm^{-2}, Cu-MWCNT composite films with relatively smooth surface morphologies were formed from each bath (a similar morphology was also seen at 0.5 A dm^{-2}). In contrast, at 5 A dm^{-2}, a smooth surface morphology was obtained only from bath D containing Cl^-. Bumpy and spherical morphologies are seen on the deposits from baths B and C, similar to the base Cu-MWCNT composite plating bath (Fig. 1b). Figure 5 shows the cathodic polarization

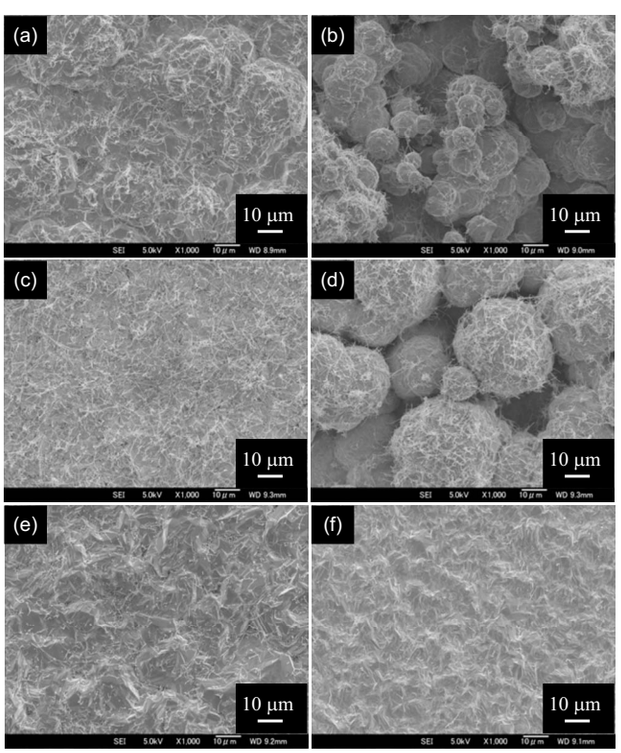

Figure 4. Surface SEM images of Cu-MWCNT composite films electrodeposited from various baths containing single additives at various current densities: (a) From bath B at 1 A dm^{-2}, (b) from bath B at 5 A dm^{-2}, (c) from bath C at 1 A dm^{-2}, (d) from bath C at 5 A dm^{-2}, (e) from bath D at 1 A dm^{-2}, and (f) from bath D at 5 A dm^{-2}.

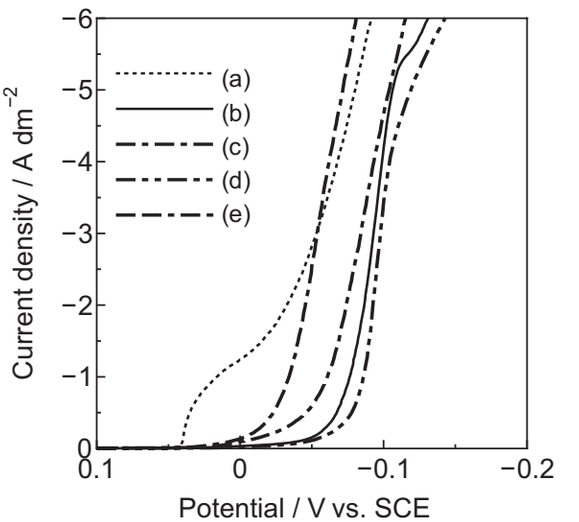

Figure 5. Cathodic polarization curves for copper deposition from (a) base bath (0.85 mol dm^{-3} $CuSO_4 \cdot 5H_2O$ + 0.55 mol dm^{-3} H_2SO_4), (b) base bath +100 ppm PA5000, (c) base bath +100 ppm PA5000 + 2 ppm SPS, (d) base bath +100 ppm PA5000 + 2 ppm JGB, and (e) base bath +100 ppm PA5000 + 50 ppm Cl^-. Scan rate is 1.7 mV s^{-1}.

curves for the cupric solutions independently containing SPS, JGB, and Cl^- as additives (corresponding to baths B, C, and D). The dotted line in Fig. 5a shows the electrodeposition behavior of copper from the base bath (0.85 mol dm^{-3} $CuSO_4 \cdot 5H_2O$ + 0.55 mol dm^{-3} H_2SO_4). The solid line in Fig. 5b shows the electrodeposition behavior of copper from the base bath + 100 ppm PA5000. The addition of PA5000 to the base bath significantly inhibited the electrodeposition of copper. The dotted–dashed line (Fig. 5c) shows the polarization curve for the base bath + 100 ppm PA5000 + 2 ppm SPS. The addition of 2 ppm SPS slightly accelerated the copper deposition compared to the base bath + 100 ppm PA5000. The two-dotted–dashed line (Fig. 5d) shows the polarization curve for the base bath + 100 ppm PA5000 + 2 ppm JGB. The addition of 2 ppm JGB slightly inhibited the copper deposition compared to the base bath + 100 ppm PA5000. The dotted–two-dashed line (Fig. 5e) shows the polarization curve for the base bath + 100 ppm PA5000 + 50 ppm Cl^-. The addition of Cl^- significantly accelerated the electrodeposition of copper compared to the base bath + 100 ppm PA5000. This acceleration effect may be related to the specific adsorption of Cl^- ions on the cathode.

Figure 6 shows surface SEM images of composite films electrodeposited at different current densities from baths E, F, and G, which contain SPS + JGB, SPS + Cl^-, and JGB + Cl^-, respectively, as additives. At 1 A dm^{-2}, the Cu-MWCNT composite films with relatively smooth surface morphologies were formed from each bath (a similar morphology was also seen at 0.5 A dm^{-2}). In contrast, at 5 A dm^{-2}, a smooth surface morphology was obtained only from bath F, containing SPS + Cl^-. Bumpy and spherical morphologies are seen on the deposits from baths E and G at 5 A dm^{-2}, similar to the base Cu-MWCNT composite plating bath (Fig. 1b). Figure 7 shows cathodic polarization curves for the cupric solutions containing two combined additives, that is, SPS + JGB, SPS + Cl^-, and JGB + Cl^- (corresponding to baths E, F, and G, respectively). In Fig. 7, the dotted line (Fig. 7a) and the solid line (Fig. 7b) show the cathodic polarization curves for the base bath and the base bath + 100 ppm PA5000, respectively, as described above. The dotted–dashed line (Fig. 7c) shows the polarization curve for the base bath + 100 ppm PA5000 + 2 ppm SPS + 2 ppm JGB. The combined addition of 2 ppm SPS + 2 ppm JGB accelerated the copper deposition at a lower current density range compared to the

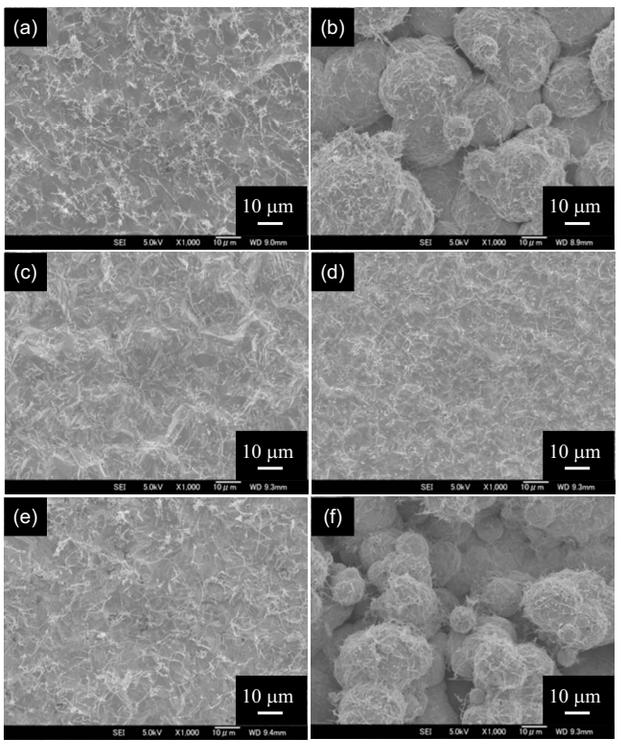

Figure 6. Surface SEM images of Cu-MWCNT composite films electrodeposited from various baths containing two additives at various current densities: (a) From bath E at 1 A dm^{-2}, (b) from bath E at 5 A dm^{-2}, (c) from bath F at 1 A dm^{-2}, (d) from bath F at 5 A dm^{-2}, (e) from bath G at 1 A dm^{-2}, and (f) from bath G at 5 A dm^{-2}.

base bath + 100 ppm PA5000. The two-dotted–dashed line (Fig. 7d) shows the polarization curve for the base bath + 100 ppm PA5000 + 2 ppm SPS + 50 ppm Cl^-. The combined addition of 2 ppm SPS + 2 ppm Cl^- significantly accelerates the

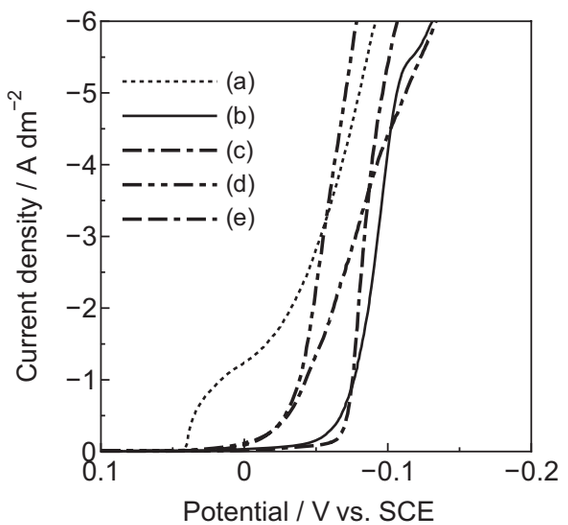

Figure 7. Cathodic polarization curves for copper deposition from (a) base bath (0.85 mol dm^{-3} $CuSO_4 \cdot 5H_2O$ + 0.55 mol dm^{-3} H_2SO_4), (b) base bath +100 ppm PA5000, (c) base bath +100 ppm PA5000 + 2 ppm SPS + 2 ppm JGB, (d) base bath +100 ppm PA5000 + 2 ppm SPS + 50 ppm Cl^-, and (e) base bath +100 ppm PA5000 + 2 ppm JGB + 50 ppm Cl^-. The scan rate used is 1.7 mV s^{-1}.

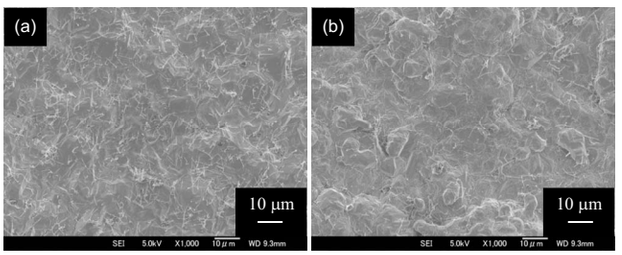

Figure 8. Surface SEM images of Cu-MWCNT composite films electrodeposited from bath H at current densities of (a) 1 and (b) 5 A dm^{-2}.

electrodeposition of copper compared to the base bath + 100 ppm PA5000. The dotted–two-dashed line (Fig. 7e) shows the polarization curve for the base bath + 100 ppm PA5000 + 2 ppm JGB + 50 ppm Cl^-. The combined addition of 2 ppm JGB + 50 ppm Cl^- slightly accelerated the copper deposition compared to the base bath + 100 ppm PA5000.

Figure 8 shows surface SEM images of the composite films electrodeposited at different current densities from bath H, which contains SPS + JGB + Cl^- as additives. The relatively smooth surface morphologies are seen at each current density (a similar morphology was also seen at 0.5 A dm^{-2}). Figure 9 shows the cathodic polarization curves for the cupric solutions containing the three combined additives corresponding to bath H. The dotted line (Fig. 9a) and the solid line (Fig. 9b) show the cathodic polarization curves for the base bath and the base bath + 100 ppm PA5000, respectively, as described above. The dashed line (Fig. 9c) shows the polarization curve for the base bath + 100 ppm PA5000 + 2 ppm SPS + 2 ppm JGB + 50 ppm Cl^-. The combined addition of 2 ppm SPS + 2 ppm JGB + 50 ppm Cl^- significantly accelerated the copper deposition compared to the base bath + 100 ppm PA5000.

Figures 4, 6, and 8 indicate that Cu-MWCNT composite films with relatively smooth surface morphologies can be obtained over a wider current density range [1(0.5)–5 A dm^{-2}] from baths D, F, and H. Meanwhile, Fig. 5, 7, and 9 indicate that the addition of Cl^-, SPS + Cl^-, and SPS + JGB + Cl^- to the base bath + 100 ppm PA5000 (corresponding to baths D, F, and H) showed a

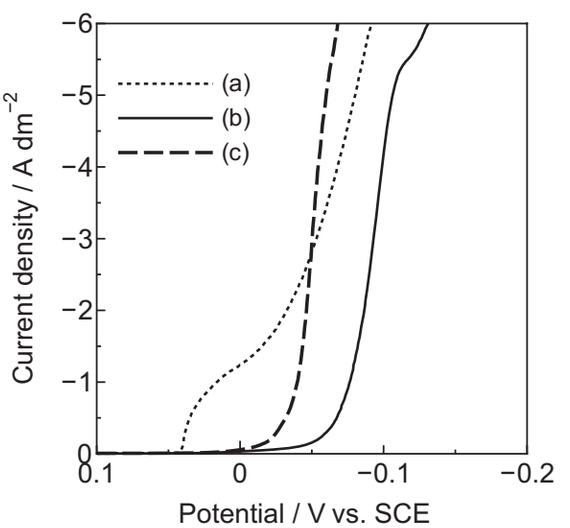

Figure 9. Cathodic polarization curves for copper deposition from (a) base bath (0.85 mol dm^{-3} $CuSO_4 \cdot 5H_2O$ + 0.55 mol dm^{-3} H_2SO_4), (b) base bath +100 ppm PA5000, and (c) base bath +100 ppm PA5000 + 2 ppm SPS + 2 ppm JGB + 50 ppm Cl^-. The scan rate is 1.7 mV s^{-1}.

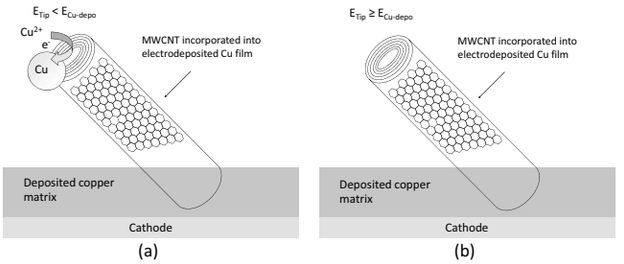

Figure 10. Schematic illustration of copper electrodeposition behavior on a protruding tip of a MWCNT incorporated in deposited copper matrix at higher current density. (a) Copper electrodeposits on the tip of the MWCNT. The potential of the tip of the MWCNT (E_{tip}) is more negative than the electrodeposition potential of copper onto the tip of the MWCNT ($E_{Cu\text{-}depo}$); this corresponds to baths B, C, E, and F, as well as the base Cu-MWCNT composite plating bath. (b) Copper does not electrodeposit on the tip of the MWCNT. The potential of the tip of the MWCNT (E_{tip}) is more positive than the electrodeposition potential of copper on the tip of the MWCNT ($E_{Cu\text{-}depo}$); this corresponds to baths D, F, and H.

significant acceleration of the copper electrodeposition compared to the base bath + 100 ppm PA5000 and other cupric solutions. The electrodeposition of copper can occur at a more positive potential in these solutions compared to other solutions at the same current density. For example, at 5 A dm^{-2}, the electrodeposition potential of copper is approximately −0.05 V in the base bath + 100 ppm PA5000 + 2 ppm SPS + 2 ppm JGB + 50 ppm Cl^-, whereas it is approximately −0.10 V in the base bath + 100 ppm PA5000 (Fig. 9). Therefore, it could be stated that the electrodeposition potentials of copper in baths D, F, and H are more positive than those in baths B, C, E, and G in the current density range of 1(0.5)–5 A dm^{-2}.

Figure 10 shows a schematic illustration of the electrodeposition behavior of copper on the Cu-MWCNT composite film at a high current density, such as 5 A dm^{-2}. If the electrodeposition of copper occurs on the ends or tips of the protruding MWCNTs, the surface morphologies of the Cu-MWCNT composite films would become bumpy, as shown in Fig. 2. For the deposition of copper onto the protruding tips of MWCNTs, the potential of the tip of the MWCNT (E_{tip}) must be more negative than the electrodeposition potential of copper onto the tip of the MWCNT ($E_{Cu\text{-}depo}$). When baths B, C, E, and G, which may not show an accelerating effect of copper electrodeposition, are used as plating baths, E_{tip} may be more negative than $E_{Cu\text{-}depo}$, resulting in the electrodeposition of copper onto the tips of the MWCNTs (Fig. 10a). Consequently, bumpy surface morphologies are generated (Fig. 2b). However, when baths D, F, and H, which show an accelerating effect of copper electrodeposition, are used as plating baths, E_{tip} may not be more negative than $E_{Cu\text{-}depo}$, resulting in no electrodeposition of copper onto the tips of the MWCNTs (Fig. 10b). In this case, therefore, relatively smooth surface morphologies are obtained (Fig. 2a).

Strictly speaking, because PA5000 is a dispersant of MWCNTs, the PA5000 must be adsorbed on the MWCNTs, resulting in a decrease in the effective concentration of PA5000 on the electrodeposition behavior of copper in the plating baths. That is, the effective concentration of PA5000 on the copper deposition behavior is lower than 100 ppm. Moreover, the adsorption of additives on the MWCNTs should also be considered. In addition, the substantial potentials of E_{tip} and $E_{Cu\text{-}depo}$ need to be discussed using the contact resistance between the MWCNT and the deposited copper matrix, the intrinsic electrical resistivity of the MWCNT, and the cathode overpotential of copper electrodeposition onto the tip of the MWCNT, which may include a charge-transfer overpotential, a diffusion overpotential, a reaction overpotential, and a crystallization overpotential.[36] We will examine these in future work.

Figure 11 shows higher magnification surface SEM images of the

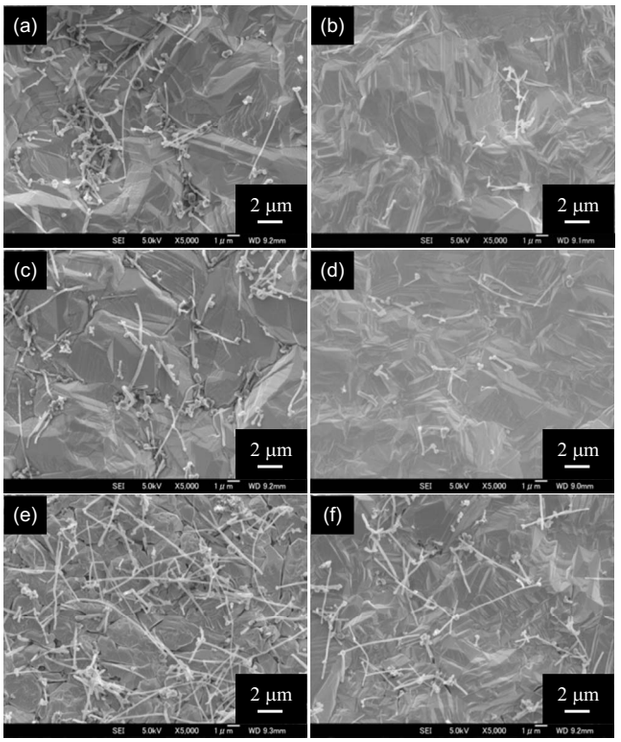

Figure 11. Higher magnification surface SEM images of Cu-MWCNT composite films electrodeposited from baths D, F, and H at various current densities: (a) From bath D at 1 A dm^{-2}, (b) from bath D at 5 A dm^{-2}, (c) from bath F at 1 A dm^{-2}, (d) from bath F at 5 A dm^{-2}, (e) from bath H at 1 A dm^{-2}, and (f) from bath H at 5 A dm^{-2}.

Cu-MWCNT composite films electrodeposited from baths D, F, and H at different current densities. Even though the MWCNTs can be seen on each of these films, the amount of MWCNTs on each film significantly varies. Very few MWCNTs are seen on the films electrodeposited from baths D (Fig. 11a and b) and F (Fig. 11c and d). In contrast, relatively more MWCNTs are seen on the films electrodeposited from bath H (Fig. 11e and f) in the current density range of 1–5 A dm^{-2}. Figure 12 shows cross-sectional SEM images of the films shown in Fig. 11. Each film has a compact microtexture and shows no voids. The dark regions are cross sections of the MWCNTs. These micrographs clearly indicate that the MWCNT content in the films electrodeposited from baths D and F is very low, whereas the MWCNT content in the films electrodeposited from bath H is relatively high at each current density. Thus, different additives not only affect the surface morphology but also affect the MWCNT content in the composite films. Among these, only bath H contains JGB as an additive. JGB is often used as a "leveler" for copper via-filling or superfilling. Li et al. reported that JGB was reduced to another product on the cathode at very low polarizing potentials in an acidic copper via-filling bath.[27] If JGB is adsorbed on the MWCNTs because JGB intrinsically possesses a positive charge, the MWCNTs may possess a positive charge. In other words, the MWCNTs then possess a positive zeta potential. This positive zeta potential might promote the incorporation of MWCNTs in the electrodeposited copper, resulting in a relatively high content of MWCNTs in the composite films. We will examine the effects of the zeta potential in detail in future work. In any case, smooth and compact Cu-MWCNT composite films containing a relatively large number of MWCNTs can be formed over a wider current density range (0.5–5 A dm^{-2}) from bath H (0.85 mol dm^{-3} $CuSO_4 \cdot 5H_2O$ + 0.55 mol dm^{-3} H_2SO_4 + 100 ppm PA5000 + 2 g dm^{-3} MWCNT + 2 ppm SPS + 2 ppm JGB + 50 ppm Cl^-).

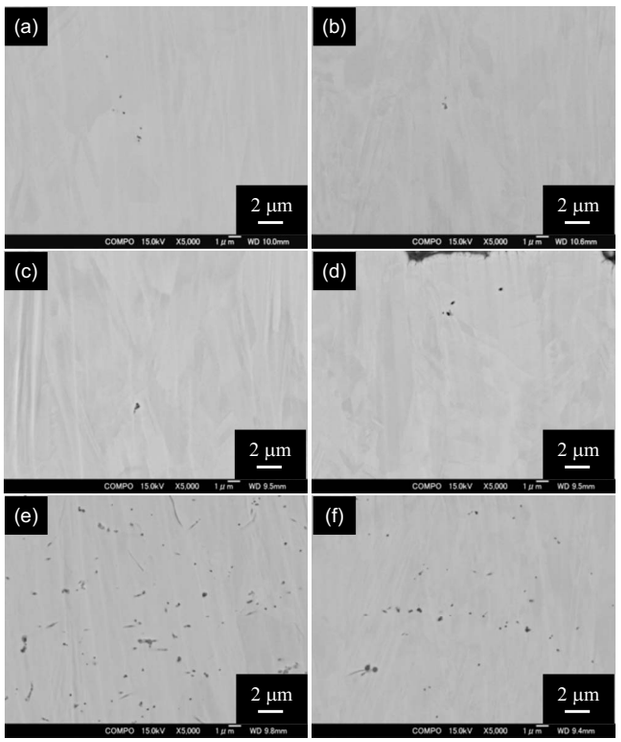

Figure 12. Cross-sectional SEM images of Cu-MWCNT composite films electrodeposited from baths D, F, and H at various current densities: (a) From bath D at 1 A dm^{-2}, (b) from bath D at 5 A dm^{-2}, (c) from bath F at 1 A dm^{-2}, (d) from bath F at 5 A dm^{-2}, (e) from bath H at 1 A dm^{-2}, and (f) from bath H at 5 A dm^{-2}.

Figure 13 shows the effects of the current density on the MWCNT content in the films electrodeposited from baths D, F, and H. The MWCNT content in the films formed from baths D and F was around 0.04 mass % (Fig. 13a and b), regardless of the current density. Meanwhile, the MWCNT content in the film formed from

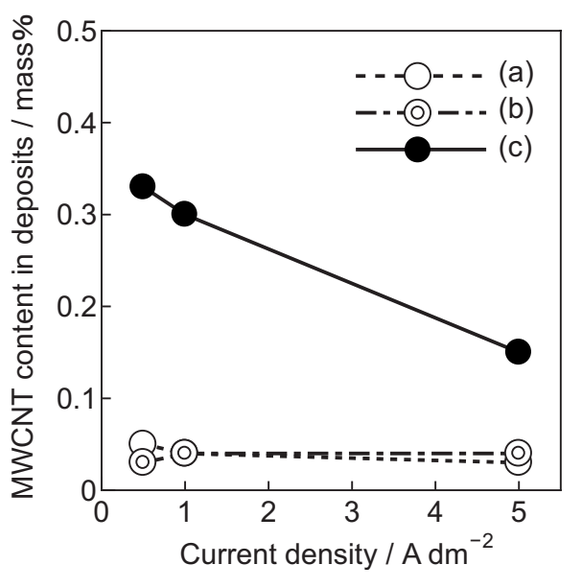

Figure 13. Effect of current density on MWCNT content in the composite films electrodeposited from various baths: (a) Bath D, (b) bath F, and (c) bath H.

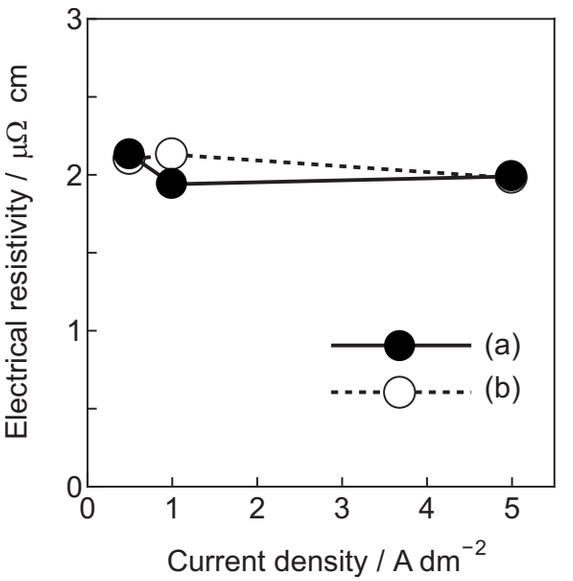

Figure 14. Effect of current density on electrical resistivity of Cu-MWCNT composite films. (a) Cu-MWCNT composite films electrodeposited from bath H and (b) copper films electrodeposited from bath H without MWCNTs.

bath H was 0.33 mass % at 0.5 A dm^{-2} and decreased with increasing current density, reaching a minimum value of 0.15 mass %, which is sufficiently higher than that of the films formed from baths D and F (Fig. 13c). These quantitative results agree with the SEM observations (Fig. 11 and 12).

Figure 14 shows the effects of current density on the electrical resistivity of the Cu-MWCNT composite film. The black circles indicate the results for the Cu-MWCNT composite films formed from bath H, whereas the white circles show the results for the copper films formed from just the bath (the same composition as bath H without MWCNTs) in comparison. The electrical resistivity of the Cu-MWCNT composite films formed from bath H was around 2 μΩ cm at each current density. This value is almost the same as that of the copper films. These results show that the addition of MWCNTs to the copper film did not significantly affect the electrical resistivity of the copper film, and the Cu-MWCNT composite films with the same electrical resistivity can be formed over a wider current density range (0.5–5 A dm^{-2}). Because the electrical resistivity of a pure copper film formed from the base bath was 1.84 μΩ cm, the electrical conductivity value of 2 μΩ cm is not very high.

Figure 15 shows the relationship between the electric field and the emission current density of the Cu-MWCNT composite films electrodeposited from bath H. The emission current was not detected from a pure copper film, whereas, as shown in Fig. 15a-c, the Cu-MWCNT composite films showed an obvious emission current. The turn-on electric field tended to slightly decrease, and the current density tended to slightly increase with increasing MWCNT content in the composite films. It is considered that the density of the protruding tips of the MWCNTs on the surface of the composite films increase with increasing MWCNT content in the composite films. Therefore, the improvement in the field emission properties may be caused by the increase in the density of the protruding tips of the MWCNTs on the surface. The turn-on electric field at 1 μA cm^{-2} and the current density at 4 V μm^{-1} of the Cu–0.33 mass % MWCNT composite film were approximately 2.4 V μm^{-1} and 100 μA cm^{-2}, respectively. Although the differences in the field emission properties were seen for the Cu-MWCNT composite films electrodeposited at different current densities, these differences were not very large. Therefore, a flat emitter fabricated using the Cu-MWCNT composite film can be expected to show almost the same

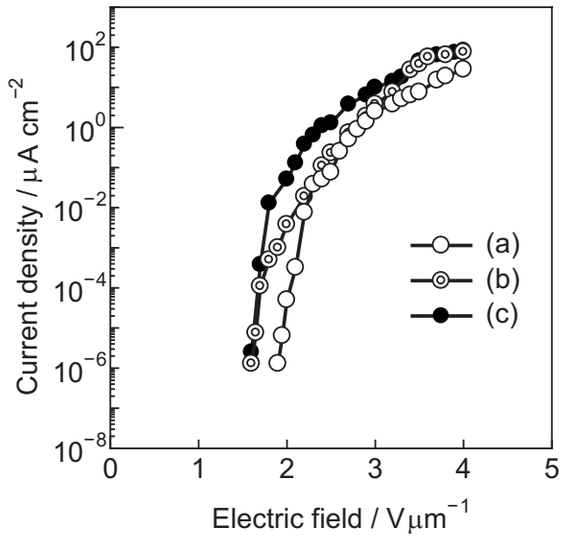

Figure 15. Relationship between electric field and emission current density of Cu-MWCNT composite films electrodeposited from bath H. (a) Cu–0.15 mass % MWCNT composite film electrodeposited at 5 A dm^{-2}, (b) Cu–0.30 mass % MWCNT composite film electrodeposited at 1 A dm^{-2}, and (c) Cu–0.33 mass % MWCNT composite film electrodeposited at 0.5 A dm^{-2}.

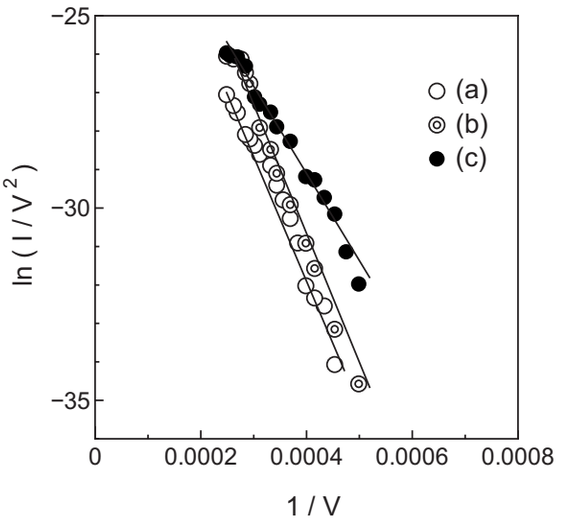

Figure 16. Fowler–Nordheim plot corresponding to Fig. 15.

field emission properties at any area on the flat emitter despite the difference in current density distribution on the cathode. This is effective and useful, for instance, in manufacturing large flat emitters for use as flat panel displays.

Generally, the field emission is described by the Fowler–Nordheim equation[37,38]

$$j = \frac{AE^2}{\phi}\exp\left(-\frac{B\phi^{3/2}}{E}\right)$$

where j is the current density, $A = 1.56 \times 10^{-6}$ A eV V^{-2}, $B = 6.83 \times 10^{7}$ eV$^{-3/2}$ V cm^{-1}, ϕ is the work function of MWCNTs, and E is the applied electric field. E is defined as $\beta V/d$ for the diode-type configuration, where V is the voltage between the anode and the emitter, d is the distance between them, and β is the field enhancement factor. If the plots of the experimental values of the electron emission current (I) as a function of the applied voltage (V) in the so-called Fowler–Nordheim coordinates, that is, ln (I/V^2) vs $1/V$, are straight lines with negative slopes, the measured emission current of the sample is the field emission current. To confirm whether the emission current of the Cu-MWCNT composite films is a real field emission current or other emission currents such as thermal emission current, the Fowler–Nordheim plots corresponding to Fig. 15 were compiled. As shown in Fig. 16, the Fowler–Nordheim plots of the Cu-MWCNT composite films were approximately straight lines with negative slopes. Therefore, the Cu-MWCNT composite films formed in the present study are real field emitters. Because the electric field at the tips of the MWCNTs are strengthened with a decreasing tip area, the field emission properties of the Cu-MWCNT composite films should be improved by using thinner MWCNTs.

Conclusions

The effects of additives on Cu-MWCNT composite films were investigated. Cu-MWCNT composite films containing a relatively large amount of MWCNTs with a smooth surface morphology were obtained over a wide current density range (0.5–5 A dm^{-2}) from a composite plating bath (0.85 mol dm^{-3} $CuSO_4 \cdot 5H_2O$ + 0.55 mol dm^{-3} H_2SO_4 + 100 ppm PA5000 + 2 g dm^{-3} MWCNTs + 2 ppm SPS + 2 ppm JGB + 50 ppm Cl^-). The electrical resistivities of these Cu-MWCNT composite films were around 2 μΩ cm. These Cu-MWCNT composite films were shown to possess good field emission properties.

Acknowledgment

This research was supported by CLUSTER (second stage) of the Ministry of Education, Culture, Sports, Science and Technology, Japan.

Shinshu University assisted in meeting the publication costs of this article.

References

1. A. Oberlin, M. Endo, and T. Koyama, *J. Cryst. Growth*, **32**, 335 (1976).
2. S. Iijima, *Nature (London)*, **354**, 56 (1991).
3. X. H. Chen, J. C. Peng, X. Q. Li, F. M. Deng, J. X. Wang, and W. Z. Li, *J. Mater. Sci. Lett.*, **20**, 2057 (2001).
4. X. H. Chen, C. S. Chen, H. N. Xiao, X. B. Liu, L. P. Zhou, S. L. Li, and G. Zhang, *Tribol. Int.*, **39**, 22 (2006).
5. L. Shi, C. F. Sun, P. Gao, F. Zhou, and W. M. Liu, *Surf. Coat. Technol.*, **200**, 4870 (2006).
6. X. H. Chen, C. S. Chen, H. N. Xiao, F. Q. Cheng, G. Zhang, and G. J. Yi, *Surf. Coat. Technol.*, **191**, 351 (2005).
7. S. Arai, M. Endo, and N. Kaneko, *Carbon*, **42**, 641 (2004).
8. S. Arai, M. Endo, S. Hashizume, and Y. Shimojima, *Electrochem. Commun.*, **6**, 1029 (2004).
9. W. Feng, S. Arai, and M. Endo, *Electrochem. Commun.*, **6**, 1021 (2004).
10. S. Arai, M. Endo, T. Sato, and A. Koide, *Electrochem. Solid-State Lett.*, **9**, C131 (2006).
11. S. Arai, T. Saito, and M. Endo, *J. Electrochem. Soc.*, **154**, D530 (2007).
12. P. C. Andricacos, C. Uzoh, J. O. Dukovic, J. Horkans, and H. Deligianni, *IBM J. Res. Dev.*, **42**, 567 (1998).
13. J. J. Kelly, C. Tian, and A. C. West, *J. Electrochem. Soc.*, **146**, 2540 (1999).
14. J. J. Kelly and A. C. West, *Electrochem. Solid-State Lett.*, **2**, 561 (1999).
15. T. P. Moffat, J. E. Bonevich, W. H. Huber, A. Stanishevsky, D. R. Kelly, G. R. Stafford, and D. Josell, *J. Electrochem. Soc.*, **147**, 4524 (2000).
16. Y. Cao, P. Taephaisitphongse, R. Chalupa, and A. C. West, *J. Electrochem. Soc.*, **148**, C466 (2001).
17. D. Josell, D. Wheeler, W. H. Huber, and T. P. Moffat, *Phys. Rev. Lett.*, **87**, 016102 (2001).
18. M. Tan and J. N. Harb, *J. Electrochem. Soc.*, **150**, C420 (2003).
19. T. P. Moffat, D. Wheeler, and D. Josell, *J. Electrochem. Soc.*, **151**, C262 (2004).
20. K. Kondo, T. Matsumoto, and K. Watanabe, *J. Electrochem. Soc.*, **151**, C250 (2004).
21. M. Hasegawa, Y. Negishi, T. Nakanishi, and T. Osaka, *J. Electrochem. Soc.*, **152**, C221 (2005).
22. W. P. Dow, H. S. Huang, M. Y. Yen, and H. C. Huang, *J. Electrochem. Soc.*, **152**, C425 (2005).
23. A. Tzanavaras, G. Young, and S. Gleixner, *J. Electrochem. Soc.*, **153**, C509 (2006).
24. J. Lee, J. Lee, J. Bae, W. Bang, K. Hong, M. H. Lee, S. G. Pyo, S. Kim, and J. G. Kim, *J. Electrochem. Soc.*, **153**, C521 (2006).
25. M. Tan, C. Guymon, D. R. Wheeler, and J. N. Harb, *J. Electrochem. Soc.*, **154**, D78 (2007).

26. C. C. Hung, W. H. Lee, S. C. Chang, K. W. Chen, and Y. L. Wang, *J. Electrochem. Soc.*, **155**, D133 (2008).
27. Y. B. Li, W. Wang, and Y. L. Li, *J. Electrochem. Soc.*, **156**, D119 (2009).
28. S. Arai and M. Endo, *Electrochem. Solid-State Lett.*, **7**, C25 (2004).
29. S. Arai and M. Endo, *Electrochem. Commun.*, **7**, 19 (2005).
30. S. Arai, T. Saito, and M. Endo, *J. Electrochem. Soc.*, Accepted for publication.
31. S. Arai and M. Endo, *Electrochem. Commun.*, **5**, 797 (2003).
32. M. Endo, Y. A. Kim, T. Hayashi, K. Nishimura, T. Matsushita, K. Miyashita, and M. S. Dresselhaus, *Carbon*, **39**, 1287 (2001).
33. S. Arai, T. Saito, and M. Endo, *Electrochem. Solid-State Lett.*, **11**, D72 (2008).
34. M. Endo, *CHEMTECH*, **18**, 568 (1998).
35. S. H. Liu, J. M. Shieh, C. Chen, K. Hensen, and S. S. Cheng, *J. Electrochem. Soc.*, **153**, C428 (2006).
36. M. Paunovic and M. Schlesinger, *Fundamentals of Electrochemical Deposition*, p. 74, John Wiley & Sons, New York (1998).
37. R. H. Fowler and L. W. Nordheim, *Proc. R. Soc. London, Ser. A*, **119**, 173 (1928).
38. J. Jiang, T. Feng, X. H. Chang, L. J. Dai, G. B. Cao, J. H. Zhang, B. Y. Jiang, X. Wang, X. H. Liu, and S. C. Zou, *Mater. Lett.*, **60**, 1085 (2006).